Journal of Mathematical Imaging and Vision manuscript No.
(will be inserted by the editor)

Morphological Amoebas are Self-Snakes

Martin Welk · Michael Breuß and Oliver Vogel

Accepted for Journal of Mathematical Imaging and Vision in September, 2010.
The final publication is available at `www.springerlink.com`.

Abstract This paper is concerned with amoeba median filtering, a structure-adaptive morphological image filter. It has been introduced by Lerallut et al. in a discrete formulation. Experimental evidence shows that iterated amoeba median filtering leads to segmentation-like results that are similar to those obtained by self-snakes, an image filter based on a partial differential equation. We establish this correspondence by analysing a space-continuous formulation of iterated amoeba median filtering. We prove that in the limit of vanishing radius of the structuring elements, iterated amoeba median filtering indeed approximates the partial differential equation of self-snakes. This result holds true under very general assumptions on the metric used to construct the amoebas. We present experiments with discrete iterated amoeba median filtering that confirm qualitative and quantitative predictions of our analysis.

M. Welk
University for Medical Informatics and Technology (UMIT), Eduard-Wallnöfer-Zentrum 1, 6060 Hall/Tyrol, Austria
Phone: +43-50-8648-3974
E-mail: martin.welk@umit.at

M. Breuß
Mathematical Image Analysis Group, Saarland University, Campus E1.1, 66041 Saarbrücken, Germany
Phone: +49-681-302-57350
Fax: +49-681-302-57342
E-mail: breuss@mia.uni-saarland.de

O. Vogel
Mathematical Image Analysis Group, Saarland University, Campus E1.1, 66041 Saarbrücken, Germany
Phone: +49-681-302-57359
Fax: +49-681-302-57342
E-mail: vogel@mia.uni-saarland.de

Keywords morphological amoebas · self-snakes · median filtering · mathematical morphology · partial differential equations

1 Introduction

Since its beginning in the 60s [24], mathematical morphology has developed into a powerful theory that provides useful operators e.g. for image denoising, structure enhancement, and shape simplification [13,28,29]. More recently, several adaptive approaches [5,23,33] have been introduced in order to support the preservation of important image structures by denoising filters.

Introduced by Lerallut et al. [22,23], morphological amoebas stand out as a class of morphological image filters in which structuring elements adapt to image structures with a maximum of flexibility. The key idea of the amoeba construction is that the structuring elements adapt locally to the variation of grey (or colour) values, also taking into account the distance to the origin pixel. Thereby, large deviations in the image values are penalised, so that the amoebas may grow around corners or along anisotropic image structures. The resulting shape then takes the role of a structuring element that can be used in conjunction with a variety of morphological filters. Our investigation in this paper concentrates on amoeba median filtering (AMF).

It is typical for the use of a classical median filter that it can be used iteratively. This is also true for amoeba median filtering. Here, iterated application can be carried out in different ways. In [22], a *pilot image* is used to steer the iterated processes via an alternating procedure. This works as follows. A smoothed version of the original image f is used for constructing amoebas for all pixels. The median filter is applied using the

corresponding structuring elements. In subsequent iterations, new amoebas are constructed in every step from the previous *filtered* image. These amoebas are then used as structuring elements to filter the *original* image f. For the purpose of the present paper, we concentrate instead on a more straightforward iterative procedure for AMF that acts analogous to classical iterated median filtering [20,31]. In each iteration, the following two steps are carried out pixelwise on the previous filtered image: (i) amoeba construction, and (ii) median filtering using the amoeba as structuring element.

For iterated median filtering with a fixed structuring element, work by Guichard and Morel [12] has brought out that, in the continuous-scale limit, it approximates the partial differential equation (PDE) $u_t = |\nabla u| \operatorname{div}\big(\nabla u / |\nabla u|\big)$, known as *(mean) curvature motion* [1]. In this sense, iterated discrete median filtering with a fixed structuring element can be understood as a specific discretisation of that PDE [18].

Iterated AMF simplifies images towards a cartoon-like appearance with homogeneous regions separated by sharp contours. Even corners are preserved fairly well, in contrast to median filtering with a fixed structuring element. Using PDE approaches, similar segmentations can be achieved e.g. by so-called self-snakes [27, 36]. These are filters that stand in close relationship to curvature motion, with the difference that the evolution is modulated by an edge-stopping function depending on the local image gradient. Thereby the displacement of edges is avoided, and edges are sharpened. In the light of Guichard and Morel's above-mentioned result it is therefore natural to ask whether there exists a similar correspondence between a continuous-scale limit case of amoeba filters and a self-snakes-like PDE.

In the following, we address this question. We prove that iterated amoeba filters can indeed be interpreted as discrete approximations of curvature-based PDE image filters. We discuss how different choices for the distance measures involved in the amoeba definition influence the limit case. In one of the settings we discuss, the self-snakes PDE is recovered.

Our results extend the framework of known correspondences between discrete and PDE formulations of morphological filters. The study of these relationships helps to gain a unified view on image filtering methods and to combine advantages of both approaches. In particular, they also allow to use amoeba procedures as discretisations of structure-adaptive PDE filters similar to [18].

Preliminary results of this research have been published in [35], where some coefficients in the derived PDEs were unfortunately flawed due to a mistake in the derivation, precluding the correct interpretation of the results.[1] In the present paper, we describe in more detail the derivation of the PDE, thereby correcting also the mistake from [35]. Moreover, while in [35] already two amoeba metrics of potential interest were introduced, most of the considerations were carried out only for the simpler of the two, namely an L_2 type (Euclidean) metric. In the present paper, the analysis is generalised to a larger class of amoeba metrics, thereby also covering the practically interesting L_1 metric case.

Related work. Median filtering in its non-adaptive form goes back to Tukey [31] and became common as a structure-preserving image filter in the 90s [10,20].

On the PDE side, (mean) curvature motion for image smoothing has been proposed by Alvarez et al. [1], already together with a "modulated" variant in which the right-hand side of the original PDE is multiplied with a decreasing function of the image gradient. Sapiro [27] proposed a modification of this idea, named *self-snakes*, in which the edge-stopping factor is placed *within* the divergence expression. While curvature motion smoothes in level-line direction only, Caselles et al. [7] defined for image interpolation purposes a process that smoothes exclusively in gradient flow line direction, called *adaptive monotone Lipschitz extension* (AMLE). The general principle to write curvature- and diffusion-based image filter PDEs as mixtures of smoothing along level line and gradient flow line directions, which is also an important ingredient of our analysis, has been established by Carmona and Zhong [6].

The representation of an image as a manifold embedded in the product space of image domain and grey-value range has been introduced in PDE-based image filtering with the so-called Beltrami framework by Kimmel et al. [19] and Yezzi [37].

Since the seminal paper by Guichard and Morel [12] further cross-relationships between discrete and PDE-based image filters have been studied. For example, van den Boomgaard [32] proved a PDE approximation result for the Kuwahara-Nagao operator [21,26]. Didas and Weickert [9] studied correspondences between adaptive averaging and a class of generalised curvature motion filters. Barash [2] and Chui and Wang [8] considered PDE limits of bilateral filters [30].

With regard to future improvements in the algorithmic realisation of amoeba filters, we mention also digital distance transforms, in particular the work by Borgefors [3,4] and Ikonen et al. [16,17].

Using a discrete filter as discretisation of a PDE by virtue of an equivalence result like [12] can also be

[1] In equation (9) of [35], a factor $\partial x / \partial z$ was omitted in both integrands, see the corrected equation (14) in the present paper and the erratum for [35] at `http://www.mia.uni-saarland.de/publications`.

seen in the context of other unconventional discretisations of continuous filters that are tailored to preserve certain important qualitative properties of PDEs. This includes, for example, mimetic discretisations [14,15] as well as so-called nonstandard schemes [25].

Structure of the paper. The paper is organised as follows. In Section 2 we describe the discrete algorithm. Our main contribution, namely the derivation of PDEs corresponding to AMF, follows in Section 3. In Section 4, we show some numerical results that illustrate the theoretical findings. The paper is finished with a conclusion in Section 5.

2 The Discrete Amoeba Construction

The basic procedure is described in Lerallut et al.'s papers [22,23]. Here, we give a brief account of the algorithm in the form we have implemented, which is slightly modified in a few points that will be pointed out in the sequel, compare also our conference paper [35].

In the following, we work with images f whose pixels are numbered by integers, such that f_i denotes the grey-value of the pixel with index i. The coordinates of this pixel are denoted by (x_i, y_i). We distinguish the initial image f from the iterated images $u^{(n)}$, where n denotes the iteration number. For starting the iterative process, we set $u^{(0)} := f$. Using the amoebas whose construction is described below as structuring elements, the standard median filter is applied.

Description of the algorithm. For each pixel i_0 with (x,y)-coordinates (x_{i_0}, y_{i_0}), an adaptive structuring element is determined as follows. We consider pixels i^* within a prescribed maximal Euclidean distance ϱ of pixel i_0. The number ϱ represents the maximal size of the shape of the amoeba, since it will also be used for limiting the allowed *amoeba distance*. For the so preselected pixels we consider paths $(i_0, i_1, \ldots, i_k \equiv i^*)$ that connect i_0 with i^* via a sequence of pixels in which each two subsequent pixels i_j, i_{j+1} are neighbours. Among all these, we determine the shortest path P with respect to the amoeba distance $L(P)$. If the amoeba distance is below ϱ for P, the pixel i^* is accepted as a member of the amoeba structuring element.

It remains to specify the amoeba distance as well as the neighbourhood relation between subsequent pixels. In [22,23], the amoeba distance is given by

$$L_L^{(n)}(P) = \sum_{m=0}^{k-1} 1 + \sigma \sum_{m=0}^{k-1} \left| u_{i_{m+1}}^{(n)} - u_{i_m}^{(n)} \right| , \tag{1}$$

where $\sigma > 0$ is a parameter that penalises large deviations in grey-value data, and each pixel is required to be in the 4-neighbourhood of its predecessor, i.e. a horizontal or vertical neighbour. Note that this definition involves the measurement of spatial distances by the L_1 distance (city-block metric), since the first sum in (1) counts the pixels in the path P (without the starting pixel i_0). Moreover, spatial and tonal distances (i.e. grey-value differences) are combined via an l_1 sum.

In our implementation, we use a metric that better approximates the Euclidean distance in space. To this end, we use 8-neighbourhoods that include horizontal, vertical, and diagonal neighbours, and use the Euclidean distance on these pixel pairs. This results in shorter paths compared to the procedure of Lerallut et al., as well, conceptually, in an improvement in terms of rotational invariance. For the way how spatial and tonal distances are combined we implement either a Euclidean sum, or an l_1 sum like in (1), which leads finally to two alternative amoeba distance measures L_2 and L_1 given by

$$L_2^{(n)}(P) = \sum_{m=0}^{k-1} \sqrt{\begin{array}{c}\left(x_{i_{m+1}} - x_{i_m}\right)^2 + \left(y_{i_{m+1}} - y_{i_m}\right)^2 \\ +\sigma^2 \left(u_{i_{m+1}}^{(n)} - u_{i_m}^{(n)}\right)^2\end{array}} \tag{2}$$

$$L_1^{(n)}(P) = \sum_{m=0}^{k-1} \left(\sqrt{\left(x_{i_{m+1}} - x_{i_m}\right)^2 + \left(y_{i_{m+1}} - y_{i_m}\right)^2} + \sigma \left| u_{i_{m+1}}^{(n)} - u_{i_m}^{(n)} \right| \right) . \tag{3}$$

While our implementation and experiments concentrate on the metrics (2), (3), in our theoretical framework these two cases will be embedded into a more general context.

We remark that the distance measurements could be improved: To better approximate the spatial Euclidean distance one could use the digital distance transforms discussed in [3], see also [4]. Alternative digital distance transforms approximating spatial-tonal Euclidean distance or L_1 distance and efficient algorithms are discussed in [16,17], for algorithms computing exact Euclidean distance see [11].

3 Space-Continuous Analysis of Amoeba Filtering

3.1 Space-Continuous Amoeba Model

For our further investigation, we need a space-continuous formulation of AMF. We base this on the representation of a (smooth) image u by its graph $\Gamma = \Gamma_{u,\sigma} := \{p(x,y) = (x, y, \sigma\, u(x,y)) \mid (x,y) \in \Omega\}$ where $\Omega \subset \mathbb{R}^2$ is the image domain, and σ a scaling parameter for grey-values as in (1)–(3). Note that

this embedding is analogous to the Beltrami framework, compare [37]. The surface Γ is equipped with a metric d which can be obtained by restricting the Euclidean metric of the embedding space $\mathbb{R}^3$, i.e.

$$d(p_1,p_2) \equiv d_2(p_1,p_2) = \min \int_0^1 \sqrt{x'(s)^2 + y'(s)^2 + \sigma^2 u'(s)^2}\,\mathrm{d}s\,, \qquad (4)$$

where the minimum is taken over all curves $[0,1] \to \Gamma$ that start in $p_1 := p(x_1,y_1)$ and end in $p_2 := p(x_2,y_2)$, and u is treated as a function of the curve parameter, $u(s) \equiv u(x(s),y(s))$ such that $u'(s) = u_x(x(s),y(s))x'(s) + u_y(x(s),y(s))y'(s)$.

Alternatively, and closer to the setting of [22], one can use an l_1 sum of the Euclidean distance in space and the grey-value distance,

$$d(p_1,p_2) \equiv d_1(p_1,p_2) = \min \int_0^1 \left(\sqrt{x'(s)^2 + y'(s)^2} + \sigma\,|u'(s)|\right)\mathrm{d}s\,. \qquad (5)$$

Of course, one could even use an l_p sum for arbitrary $p \geq 1$; this would include in the limit $p \to \infty$ an amoeba metric that measures the maximum of the spatial and weighted tonal distance. For our theoretical considerations, we will use as the most general setting a metric

$$d(p_1,p_2) \equiv d_\varphi(p_1,p_2) = \min \int_0^1 \varphi\left(\sqrt{x'(s)^2 + y'(s)^2}, \sigma\,|u'(s)|\right)\mathrm{d}s\,, \qquad (6)$$

where φ is a homogeneous C^2 function of degree 1, strictly increasing in both variables, and fulfils the triangle inequality $\varphi(s+v,t+w) \leq \varphi(s,t) + \varphi(v,w)$.

One step of amoeba filtering then reads as follows. For a given location (x_0,y_0) in the image domain, an amoeba structuring element $\mathcal{A}(x_0,y_0)$ is constituted by all locations (x,y) for which $d(p(x_0,y_0),p(x,y))$ does not exceed a given radius ϱ. Typical shapes of amoeba structuring elements with the metrics d_2 and d_1 are shown in Figure 1. It is worth noticing that with the metric $d \equiv d_2$ from (4) the boundary of $\mathcal{A}(x_0,y_0)$ crosses the level line through (x_0,y_0) orthogonally and smoothly, while e.g. with $d \equiv d_1$ as given by (5) it has kinks at the intersection points, giving the structuring element a digonal overall shape in contrast to the elliptical contour with (4).

Once the structuring element has been constructed, the median of all grey-values of the unfiltered image within the structuring element is taken, i.e. the value μ whose level line (the curve along which $u(x,y) = \mu$ holds) cuts $\mathcal{A}(x_0,y_0)$ into two parts of equal area. In the filtered image, μ becomes the new grey-value at location (x_0,y_0).

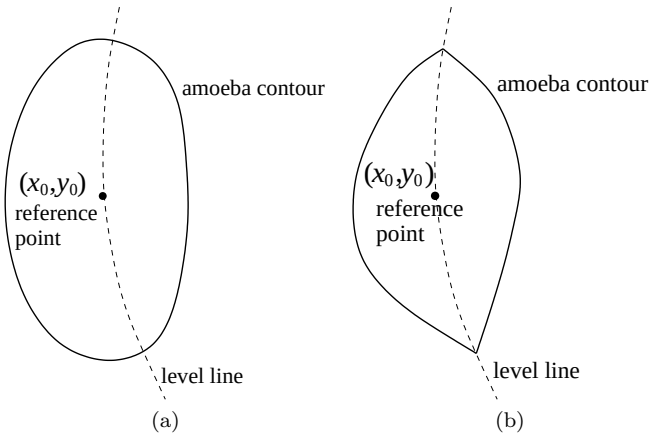

Fig. 1 Amoeba structuring elements. **(a)** Typical amoeba with metric $d \equiv d_2$ from (4). **(b)** Typical amoeba with metric $d \equiv d_1$ from (5).

3.2 Derivation of a Partial Differential Equation for Amoeba Median Filtering

We analyse the amoeba median filter now in a manner similar to Guichard and Morel's approach [12], assuming that the amoeba metric is of type (6).

Without loss of generality, we assume that we are dealing with the location $(x_0,y_0) = (0,0)$. We assume further that $u(x_0,y_0) = 0$, and that the image gradient at (x_0,y_0) is given by $\nabla u(x_0,y_0) = (\alpha/\sigma, 0)^{\mathrm{T}}$ with some positive α. Then $\sigma\,u$ possesses the Taylor expansion

$$\sigma\,u(x,y) = \alpha x + \beta x^2 + \gamma xy + \delta y^2 + \mathcal{O}(\varrho^3) \qquad (7)$$

within $\mathcal{A} = \mathcal{A}(x_0,y_0)$, where we have used that $x,y = \mathcal{O}(\varrho)$.

Consider now a value $z = \mathcal{O}(\varrho)$. We are interested in the level line of u corresponding to the grey-value z/σ, restricted to $\mathcal{A}$. On this line, $\sigma\,u(x,y) = z$ holds. Due to the prescribed gradient direction of u, level lines of u within $\mathcal{A}$ are roughly oriented in y direction. We can therefore express the level line by writing x as a function of y. To this end, we read $\sigma\,u(x,y) = z$ as a quadratic equation for x with the solutions

$$x_{1,2} = \frac{1}{2\beta}\Big(-\alpha - \gamma y \pm \sqrt{(\alpha+\gamma y)^2 - 4\beta(\delta y^2 - z)}\Big) + \mathcal{O}(\varrho^3)\,. \qquad (8)$$

We drop the "$-$" solution which is outside $\mathcal{A}$ if ϱ is small enough, and use the Taylor expansion $\sqrt{1+v} =$

$1+\frac{1}{2}v-\frac{1}{8}v^2+\mathcal{O}(v^3)$ to obtain

$$\begin{aligned} x &= \frac{1}{2\beta}\Bigg(-\alpha-\gamma y \\ &\qquad +\alpha\sqrt{1+\frac{2\gamma}{\alpha}y+\frac{4\beta}{\alpha^2}z+\frac{\gamma^2}{\alpha^2}y^2-\frac{4\beta\delta}{\alpha^2}y^2}\Bigg)+\mathcal{O}(\varrho^3) \\ &= \frac{1}{2\beta}\Bigg(-\alpha-\gamma y+\alpha+\gamma y+\frac{2\beta z}{\alpha}+\frac{\gamma^2}{2\alpha}y^2-\frac{2\beta\delta}{\alpha}y^2 \\ &\qquad -\frac{\gamma^2}{2\alpha}y^2-\frac{2\beta\gamma}{\alpha^2}yz-\frac{2\beta^2}{\alpha^3}z^2\Bigg)+\mathcal{O}(\varrho^3) \end{aligned} \tag{9}$$

and thus

$$x=x(y)=x(y,z)=\left(\frac{z}{\alpha}-\frac{z^2\beta}{\alpha^3}\right)-\frac{z\gamma}{\alpha^2}y-\frac{\delta}{\alpha}y^2+\mathcal{O}(\varrho^3)\ . \tag{10}$$

We will now compute the length of the level line segment within $\mathcal{A}$ because it contributes to the weight with which the value $u=z/\sigma$ enters the computation of the median μ. The end points of this segment are obtained by equating $d_\varphi(p(x_0,y_0),p(x(y),y))$ to ϱ.

Approximating d_φ by the corresponding distance within $\mathbb{R}^3$, this equation becomes $\varphi\left(\sqrt{x(y)^2+y^2},|z|\right)=\varrho$. Using the homogeneity of φ we can write $\varphi(v,w)=w\varphi(\frac{v}{w},1)=:w\psi(\frac{v}{w})$. Thus we have $|z|\,\psi\left(\frac{\sqrt{x(y)^2+y^2}}{|z|}\right)=\varrho$, and finally

$$x(y)^2+y^2=z^2\psi^{-2}\left(\frac{\varrho}{|z|}\right)\ , \tag{11}$$

where ψ^{-2} denotes the square of the inverse function of ψ.

We substitute (10) into the condition. Since $y,z=\mathcal{O}(\varrho)$, we obtain

$$\begin{aligned} &\left(1-\frac{2\delta}{\alpha^2}z\right)y^2-\frac{2\gamma}{\alpha^3}z^2y+\left(\frac{1}{\alpha^2}-\psi^{-2}\left(\frac{\varrho}{|z|}\right)\right)z^2 \\ &\qquad -\frac{2\beta}{\alpha^4}z^3+\mathcal{O}(\varrho^4)=0\ , \end{aligned} \tag{12}$$

a quadratic equation for y. For its two solutions y_1, y_2 one easily checks that $y_1,y_2=\mathcal{O}(\varrho)$ and $\frac{y_1+y_2}{2}=\mathcal{O}(\varrho^2)$.

The difference $|y_1-y_2|$ yields up to $\mathcal{O}(\varrho^3)$ the desired length $L(z)$ of the level line segment within $\mathcal{A}$. Using the solution rule for quadratic equations and keeping track of the order of higher order terms, we find that

$$\begin{aligned} L(z) &= 2\,|z|\sqrt{\psi^{-2}\left(\frac{\varrho}{|z|}\right)-\frac{1}{\alpha^2}}\times \\ &\quad\times\left(1+\frac{\delta}{\alpha^2}z+\frac{\beta}{\alpha^4\psi^{-2}\left(\frac{\varrho}{|z|}\right)-\alpha^2}z\right)+\mathcal{O}(\varrho^3)\ . \end{aligned} \tag{13}$$

To determine the median μ, we consider the equation

$$\int_{Z_-}^{\sigma\mu}L(\zeta)\,\frac{\partial x}{\partial z}(\zeta)\,\mathrm{d}\zeta=\int_{\sigma\mu}^{Z_+}L(\zeta)\,\frac{\partial x}{\partial z}(\zeta)\,\mathrm{d}\zeta\ , \tag{14}$$

where Z_+ and Z_- are the smallest positive and largest negative values for which $L(Z_+)=L(Z_-)=0$, and the derivative $\frac{\partial x}{\partial z}(\zeta)=\frac{\partial x}{\partial z}(\frac{y_1+y_2}{2},\zeta)$ is taken at the midpoint of the corresponding level line segment, $\frac{y_1+y_2}{2}=\mathcal{O}(\varrho^2)$. To interpret (14), we notice that each side integrates the lengths $L(\zeta)$ of level line segments over some range of grey-values, weighted with the inverse density $\frac{\partial x}{\partial z}(\zeta)$ of these level lines. As a consequence, each integral measures the area of the portion of the structuring element with grey-values in its integration domain, and (14) as a whole expresses the condition that the portions with grey-values below and above μ have equal area, which is exactly the characterisation of the median.

From (10) it follows that

$$\frac{\partial x}{\partial z}(\zeta)=\frac{1}{\alpha}-\frac{2\beta}{\alpha^3}\zeta+\mathcal{O}(\varrho^2)\ . \tag{15}$$

For the integration bounds in (14) one has $Z_+,-Z_-=Z_*+\mathcal{O}(\varrho^3)$ with $Z_*=\varrho/\psi(1/\alpha)$ (remember that $\alpha>0$).

Provided that $\mu=\mathcal{O}(\varrho^2)$, the equality (14) can then be transformed into

$$\begin{aligned} &\int_0^{Z_*}\left(L(\zeta)\cdot\frac{\partial x}{\partial z}(\zeta)-L(-\zeta)\cdot\frac{\partial x}{\partial z}(-\zeta)\right)\mathrm{d}\zeta \\ &=2\sigma\mu L(0)\cdot\frac{\partial x}{\partial z}(0)+\mathcal{O}(\varrho^4)\ . \end{aligned} \tag{16}$$

We multiply with α in order to eliminate the factor $\frac{\partial x}{\partial z}(0)=\frac{1}{\alpha}$, and insert (15) to obtain

$$\begin{aligned} &\int_0^{Z_*}\left(L(\zeta)\left(1-\frac{2\beta}{\alpha^2}\zeta\right)-L(-\zeta)\left(1+\frac{2\beta}{\alpha^2}\zeta\right)\right)\mathrm{d}\zeta \\ &=2\sigma\mu L(0)+\mathcal{O}(\varrho^4)\ . \end{aligned} \tag{17}$$

Up to higher order terms the left-hand side equals

$$\begin{aligned} &\frac{4(\delta-2\beta)}{\alpha^2}\int_0^{Z_*}\zeta^2\sqrt{\psi^{-2}\left(\frac{\varrho}{|\zeta|}\right)-\frac{1}{\alpha^2}}\,\mathrm{d}\zeta \\ &\qquad+\frac{4\beta}{\alpha^4}\int_0^{Z_*}\frac{\zeta^2}{\sqrt{\psi^{-2}\left(\frac{\varrho}{|\zeta|}\right)-\frac{1}{\alpha^2}}}\,\mathrm{d}\zeta \\ &\qquad=\frac{4\varrho^3(\delta-2\beta)}{\alpha^2\psi^3(1/\alpha)}I_1(\alpha)+\frac{4\varrho^3\beta}{\alpha^4\psi^3(1/\alpha)}I_2(\alpha)\ , \end{aligned} \tag{18}$$

where the two integrals

$$I_1(\alpha) := \int_0^1 \xi^2 R_\psi(\xi,\alpha)\,\mathrm{d}\xi \tag{19}$$

$$I_2(\alpha) := \int_0^1 \frac{\xi^2}{R_\psi(\xi,\alpha)}\,\mathrm{d}\xi \tag{20}$$

depend on the expression

$$R_\psi(\xi,\alpha) := \sqrt{\psi^{-2}\left(\frac{1}{\xi}\psi\left(\frac{1}{\alpha}\right)\right) - \frac{1}{\alpha^2}}\ . \tag{21}$$

Together with $L(0) = 2\varrho + \mathcal{O}(\varrho^3)$, this implies

$$\mu = \frac{\varrho^2}{3\sigma}\left(\frac{3\delta I_1(\alpha)}{\alpha^2\psi^3(1/\alpha)} + \frac{3\beta(I_2(\alpha) - 2\alpha^2 I_1(\alpha))}{\alpha^4\psi^3(1/\alpha)}\right) + \mathcal{O}(\varrho^3) \tag{22}$$

which by virtue of (7) can be restated in terms of spatial derivatives of u as

$$\begin{aligned}\mu = \frac{\varrho^2}{6}\Bigg(&\frac{3u_{yy}I_1(\sigma\,u_x)}{(\sigma\,u_x)^2\psi^3(\sigma^{-1}u_x^{-1})}\\ &+ \frac{3u_{xx}(I_2(\sigma\,u_x) - 2(\sigma\,u_x)^2 I_1(\sigma\,u_x))}{(\sigma\,u_x)^4\psi^3(\sigma^{-1}u_x^{-1})}\\ &+ \mathcal{O}(\varrho)\Bigg)\ .\end{aligned} \tag{23}$$

We have therefore obtained a result of the same type as the equivalence from [12]:

One step of amoeba median filtering acts approximately like one time step of an explicit scheme for the PDE

$$u_t = g(|\nabla u|)u_{\xi\xi} + h(|\nabla u|)u_{\eta\eta} \tag{24}$$

with time step size $\tau = \varrho^2/6$, where g and h are two weight functions given by

$$g(s) = \frac{3I_1(\sigma s)}{(\sigma s)^2\psi^3(1/(\sigma s))}\ , \tag{25}$$

$$h(s) = \frac{3I_2(\sigma s)}{(\sigma s)^4\psi^3(1/(\sigma s))} - 2g(s)\ . \tag{26}$$

On the right-hand side, second order derivatives are taken in the directions of the normalised gradient vector $\eta := \nabla u/|\nabla u|$ and the perpendicular vector $\xi := \eta^\perp$, the tangential vector of the local level line of u.

When ϱ tends to zero, the iterated amoeba median filter therefore converges to the PDE (24). The first summand of the right-hand side of (24) can obviously be interpreted as right-hand side of curvature motion $u_t = u_{\eta\eta}$ multiplied by an edge-stopping factor $g(|\nabla u|)$. The second summand corresponds to an AMLE evolution [7] weighted with $h(|\nabla u|)$. However, as h takes negative values, this term represents rather an edge-enhancing backward AMLE, i.e. a one-dimensional backward diffusion process.

While for general functions ψ the integrals I_1 and I_2 may not be solvable in closed form, it is possible to compute these integrals, and thereby the weight functions g and h, numerically and thereby to implement a numerical scheme for the evolution PDE (24). In calculating the integrals, however, care must be taken of the (weak) singularity of the integrands at $\xi = 1$. The weight functions g and h for important special cases of the amoeba metric will be discussed in Subsection 3.3. Here we continue by establishing a further important relationship between the two functions.

It is easy to show that the derivative of the integrand of I_1 w.r.t. α is bounded over the product $[a,b]\times[0,1]$ of closed intervals $[a,b]$ $(0 < a < b)$ for α and $[0,1]$ for ξ such that it is uniformly continuous. It follows further that its integral is uniformly convergent w.r.t. α. As a consequence, one can compute $I_1'(\alpha)$ by differentiating the integrand of (19), which yields

$$\begin{aligned}I_1'(\alpha) &= \int_0^1 \xi^2 \frac{\partial}{\partial\alpha} R_\psi(\xi,\alpha)\,\mathrm{d}\xi\\ &= \frac{\xi\,\psi^{-3}\left(\frac{1}{\xi}\,\psi\left(\frac{1}{\alpha}\right)\right)\psi'\left(\frac{1}{\alpha}\right)}{\alpha^2\,R_\psi(\xi,\alpha)\,\psi'\left(\psi^{-1}\left(\frac{1}{\xi}\,\psi\left(\frac{1}{\alpha}\right)\right)\right)}\ .\end{aligned} \tag{27}$$

Using (25) with the quotient rule, (26) and (27) gives

$$sg'(s) - h(s) = \frac{3\psi'\left(\frac{1}{\sigma s}\right)}{(\sigma s)^3\psi^4\left(\frac{1}{\sigma s}\right)} I_3(\sigma s) \tag{28}$$

where I_3 stands for the integral

$$\begin{aligned}I_3(\alpha) := \int_0^1 \Bigg(&3\xi^2 R_\psi(\xi,\alpha)\\ &- \frac{\xi\psi^{-1}\left(\frac{1}{\xi}\psi\left(\frac{1}{\alpha}\right)\right)\psi\left(\frac{1}{\alpha}\right)}{\psi'\left(\psi^{-1}\left(\frac{1}{\xi}\psi\left(\frac{1}{\alpha}\right)\right)\right)R_\psi(\xi,\alpha)}\Bigg)\,\mathrm{d}\xi\ .\end{aligned} \tag{29}$$

To evaluate this definite integral, we make use of the antiderivative (primitive)

$$\begin{aligned}\int \left(3\xi^2 R_\psi(\xi,\alpha) - \frac{\xi\psi^{-1}\left(\frac{1}{\xi}\psi\left(\frac{1}{\alpha}\right)\right)\psi\left(\frac{1}{\alpha}\right)}{\psi'\left(\psi^{-1}\left(\frac{1}{\xi}\psi\left(\frac{1}{\alpha}\right)\right)\right)R_\psi(\xi,\alpha)}\right)\mathrm{d}\xi\\ = \xi^3 R_\psi(\xi,\alpha)\end{aligned} \tag{30}$$

and find $I_3(\alpha) = R_\psi(1,\alpha)$. By the definition (21) of R_ψ we have $R_\psi(1,\alpha) = \sqrt{\psi^{-2}(\psi(1/\alpha) - 1/\alpha^2} =$

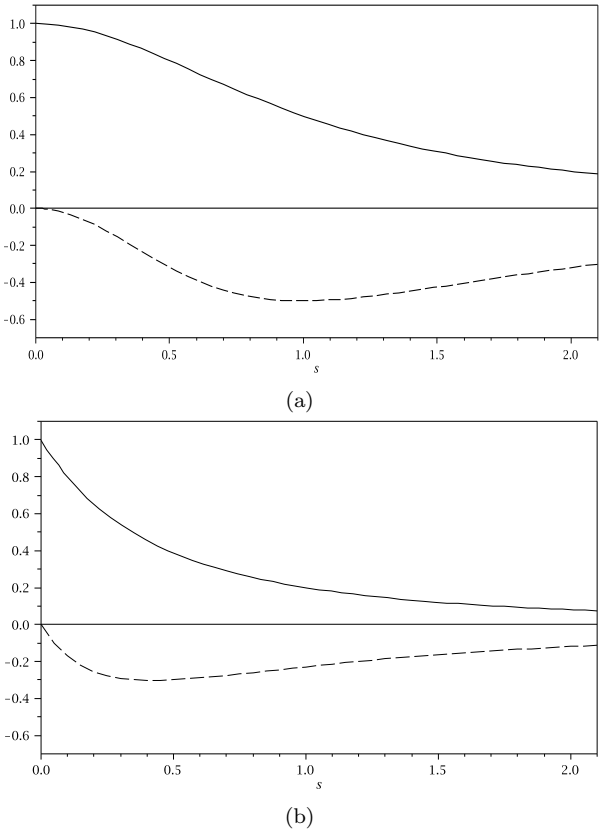

Fig. 2 Edge-stopping functions in PDEs approximated by iterated amoeba median filtering. For visualisation, σ is fixed to 1. **(a)** Weight functions $g(s) = \left(1 + s^2\right)^{-1}$ for the curvature motion term (solid line), $h(s) = -2s^2\left(1 + s^2\right)^{-2}$ for the shock term (dashed line) from the PDE (24) using the Euclidean amoeba metric (4). **(b)** Corresponding weight functions for the amoeba metric (5).

$\sqrt{1/\alpha^2 - 1/\alpha^2} = 0$, which implies $I_3(\alpha) = 0$ and, by virtue of (28), finally $sg'(s) = h(s)$.

With the help of this equality, the second summand in (24) can be rewritten as $|\nabla u|\, g'(|\nabla u|)\, u_{\eta\eta}$. The latter expression transforms further into $\langle \nabla g, \nabla u \rangle$.

As a result, we see that (24) is nothing else than the self-snakes PDE [27,36]

$$\begin{aligned} u_t &= |\nabla u| \operatorname{div} \left(g(|\nabla u|) \frac{\nabla u}{|\nabla u|} \right) \\ &= g(|\nabla u|) u_{\xi\xi} + \langle \nabla g(|\nabla u|), \nabla u \rangle \end{aligned} \tag{31}$$

with the edge-stopping function g defined by (25).

3.3 Important Special Cases

While we have obtained the equivalence result in Section 3.2 in the fairly general setting of the amoeba metric (6), we believe that the Euclidean and L_1 amoeba metric as given by (4) and (5), respectively, are the most

Fig. 3 The ***Cameraman*** experiment. **(a)** Original image. **(b)** Iterated median filtering of (a), 3×3 stencil, 40 iterations. **(c)** Iterated amoeba median filtering of (a) with Euclidean amoeba distance, $\varrho = 10$, $\sigma = 0.25$, 4 iterations.

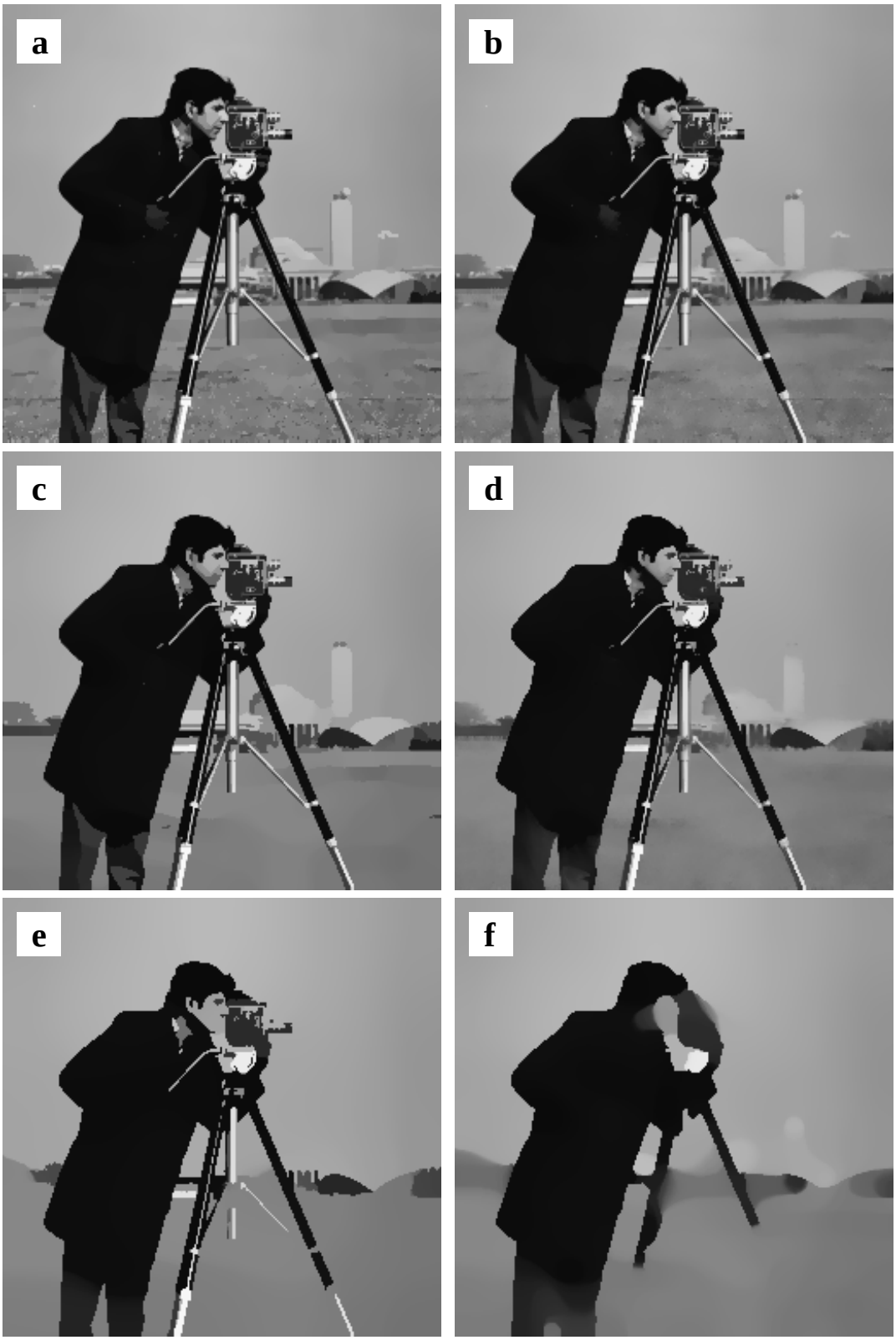

Fig. 4 Iterated amoeba median filtering of *cameraman* image with different parameters. The Euclidean amoeba distance was used throughout this figure. **Top row: (a)** $\varrho = 5$, $\sigma = 0.25$, 4 iterations. **(b)** $\varrho = 10$, $\sigma = 0.25$, 1 iteration. **Middle row: (c)** $\varrho = 10$, $\sigma = 0.25$, 4 iterations. **(d)** $\varrho = 20$, $\sigma = 0.25$, 1 iteration. iterations. **Bottom row: (e)** $\varrho = 20$, $\sigma = 0.25$, 4 iterations. **(f)** $\varrho = 10$, $\sigma = 0.05$, 4 iterations.

interesting cases for practical use. We will therefore now discuss the application of the general derivation and results to these two cases.

Looking first at the Euclidean amoeba metric (4), we see that it corresponds to setting $\varphi(v,w) = \sqrt{v^2+w^2}$ in (6). The corresponding function ψ is given by $\psi(v) = \sqrt{1+v^2}$. In this case, the integrals I_1 and I_2 are easy to solve in closed form:

$$I_1(\alpha) = \sqrt{1+\frac{1}{\alpha^2}} \int_0^1 \xi\sqrt{1-\xi^2}\,\mathrm{d}\xi = \frac{1}{3}\sqrt{1+\frac{1}{\alpha^2}} \tag{32}$$

$$I_2(\alpha) = \frac{1}{\sqrt{1+\frac{1}{\alpha^2}}} \int_0^1 \frac{\xi^3}{\sqrt{1-\xi^2}}\,\mathrm{d}\xi = \frac{2}{3\sqrt{1+\frac{1}{\alpha^2}}}\,. \tag{33}$$

The weight functions in (24) are now given by

$$g(s) = \frac{1}{1+s^2}\,, \qquad h(s) = \frac{-2s^2}{(1+s^2)^2} \tag{34}$$

for which $sg'(s) = h(s)$ is evident. Both functions are displayed in Figure 2(a). Note that in this case the edge-stopping function in the self-snakes PDE (31) is of Perona-Malik type with threshold $1/\sigma$.

In the case of the L_1 amoeba metric (5), we have $\varphi(v,w) = v+w$ and thus $\psi(v) = 1+v$. Here, the integrals I_1 and I_2 are best evaluated numerically. The resulting weight functions g, h are shown in Figure 2(b). The most prominent difference to the Euclidean case is the faster decay of the edge-stopping function g from its start at $g(0) = 1$ which means that small contrast stronger dampens the evolution.

4 Experiments

We present two experiments that confirm the behaviour suggested by the analytical results from the previous section.

The *Cameraman* experiment. We use first an image with a moderate amount of structures of different sizes in order to investigate the effect of the different parameters of the amoeba median filtering algorithm, see Figure 4, and to compare results against self-snakes, see Figure 5.

Figure 3(a) shows the original image. Subfigure (b) depicts the steady state of standard median filtering with a fixed (3×3) structuring element. As usual with median filtering, the shape of edges is rounded, and small structures, even of high contrast, are lost. The use of a larger non-adaptive structuring element will distort the shape of important image features.

Fig. 5 The ***Cameraman*** experiment with self-snakes. An edge-stopping function of Perona-Malik type (corresponding to the Euclidean amoeba metric) is used. **(a)** Self-snakes filtering of Fig. 3(a), $\sigma = 0.25$, time step 0.25, 67 iterations. **(b)** Same as in (a) but 267 iterations. **(c)** Same as in (b) but $\sigma = 0.05$.

In contrast, iterated AMF using the L_2 amoeba distance, Figure 3(c), simplifies preferably structures of low contrast, and retains more accurately the shape of objects.

In Figure 4 we compare the results of iterated AMF using the L_2 amoeba distance together with varying parameters. We start with a relatively strong penalisation of grey-value differences given by $\sigma = 0.25$, see (a–e). This leads to a visible image simplification in which almost flat image regions are flattened even more. Edges are sharpened but stay fairly well in place.

The degree of simplification naturally increases with the number of iterations with fixed amoeba radius, as from (b) to (c) and from (d) to (e), and with the amoeba radius, as from (a) via (c) to (e). At the same time, it can be observed that four iterations of AMF with a given amoeba radius correspond reasonably well to a single iteration with double amoeba radius, see the image pairs (a)–(b) and (c)–(d). This matches the quadratic relationship $\tau = \varrho^2/6$ between amoeba radius and evolution time of our PDE equivalence result.

When a very small σ is used, as in Figure 4(f), image contrast has little influence on the amoeba shapes such that the filter gets close to a non-adaptive median filter with large structuring elements. The typical rounding of corners and disappearance of small-scale structures can be observed well. Translating to the approximated self-snakes evolution, the edge-stopping function now takes values close to 1, implying a smoothing behaviour very similar to curvature motion.

For comparison, Figure 5 displays results of numerical evaluation of the self-snakes PDE (31) with Euclidean (Perona-Malik) edge-stopping function $g(s) = (1+\sigma^2 s^2)^{-1}$. An explicit time-stepping scheme was used wherein the curvature-motion component $g(|\nabla u|)u_{\xi\xi}$ was discretised using central differences, while the backward AMLE contribution was discretised by an upwind-like discretisation.

The parameters for Figure 5(a) have been adjusted to match those of the AMF experiment in Figure 4(b). Figure 5(b) is adjusted to match Figure 4(c) or (d). Finally, for Figure 5(c) the parameters of Figure 4(f) have been translated to the self-snakes setting. Despite some deviations in details, the overall similarity is clearly visible. As a rule, small details are handled worse by the conventional PDE discretisation in Figure 5 which can be attributed to the inevitable blurring effect of discretising derivatives.

In order to rely not only on visual judgements, we compare AMF and self-snakes filtering results also by quantitative measurements. One should be aware, however, that no known error measure is able to represent adequately the visual similarity judgement of humans. It is also important to note that the image filters under consideration tend to create images consisting of homogeneous regions separated by sharp contours, where small shifts of contours involve large grey-value changes in many pixels in spite of little visual significance.

The first measure is the *mean absolute error (MAE)*. For two images $u = (u_{i,j})$, $v = (v_{i,j})$ with a size of N pixels it is given by

$$\mathrm{MAE}(u,v) := \frac{1}{N}\sum_{(i,j)} |u_{i,j} - v_{i,j}| \ . \tag{35}$$

Being based on strictly local grey-value comparison, MAE is prone to over-emphasise the above-mentioned small contour shifts. Therefore we complement MAE by a second measure which tries to mitigate this effect by using statistics within small neighbourhoods, the *mean structural similarity index (MSSIM)* [34]. It is defined as the average of the *structural similarity index (SSIM)* over all windows $\mathcal{W}$ of a prescribed size w within the image domain. SSIM itself is computed as

$$\mathrm{SSIM}_{\mathcal{W}}(u,v) := \frac{(2\mu_u\mu_v + c_1)(2\sigma_{uv} + c_2)}{(\mu_u^2 + \mu_v^2 + c_1)(\sigma_u^2 + \sigma_v^2 + c_2)} \tag{36}$$

where μ_u, μ_v denote the averages of u, v, respectively, and σ_u, σ_v the standard deviations of u, v within $\mathcal{W}$, and σ_{uv} the covariance of u and v within W. The constants c_1 and c_2 are chosen as $0.01 \cdot 255^2$ and $0.03 \cdot 255^2$, respectively, for images with grey-value range $[0, 255]$. We fix the window size to $w = 4$. MSSIM takes values between -1 and $+1$ where $+1$ indicates perfect match.

Table 1 shows the MAE and MSSIM values for the five AMF images from Figure 4(b–f) versus the three self-snakes results from Figure 5, and of all these images versus the original cameraman image from Figure 3. It can be seen that also in terms of the quantitative measurements the filtering results that correspond theoretically are in comparatively good agreement. A deviation is seen for AMF results from Figure 4(c) and (d) which according to the measurements seem to be slightly closer to Figure 5(a) than (b). This is, however, not supported by the visual impression.

The *Head* experiment. In our second experiment (Figure 6) we use an MR image of a human head which abounds in details of different contrast and scale. The original image is shown in Subfigure (a), a non-adaptive median filter result in (b). In (c) and (d) iterated AMF results both with L_2 and L_1 amoeba distance are displayed. It can be seen that both distance measures lead to similar results. Moreover, we observe even clearer than in the *Cameraman* experiment the good quality of segmentation-type filtering that is achieved in spite of the relative simplicity of the filtering approach.

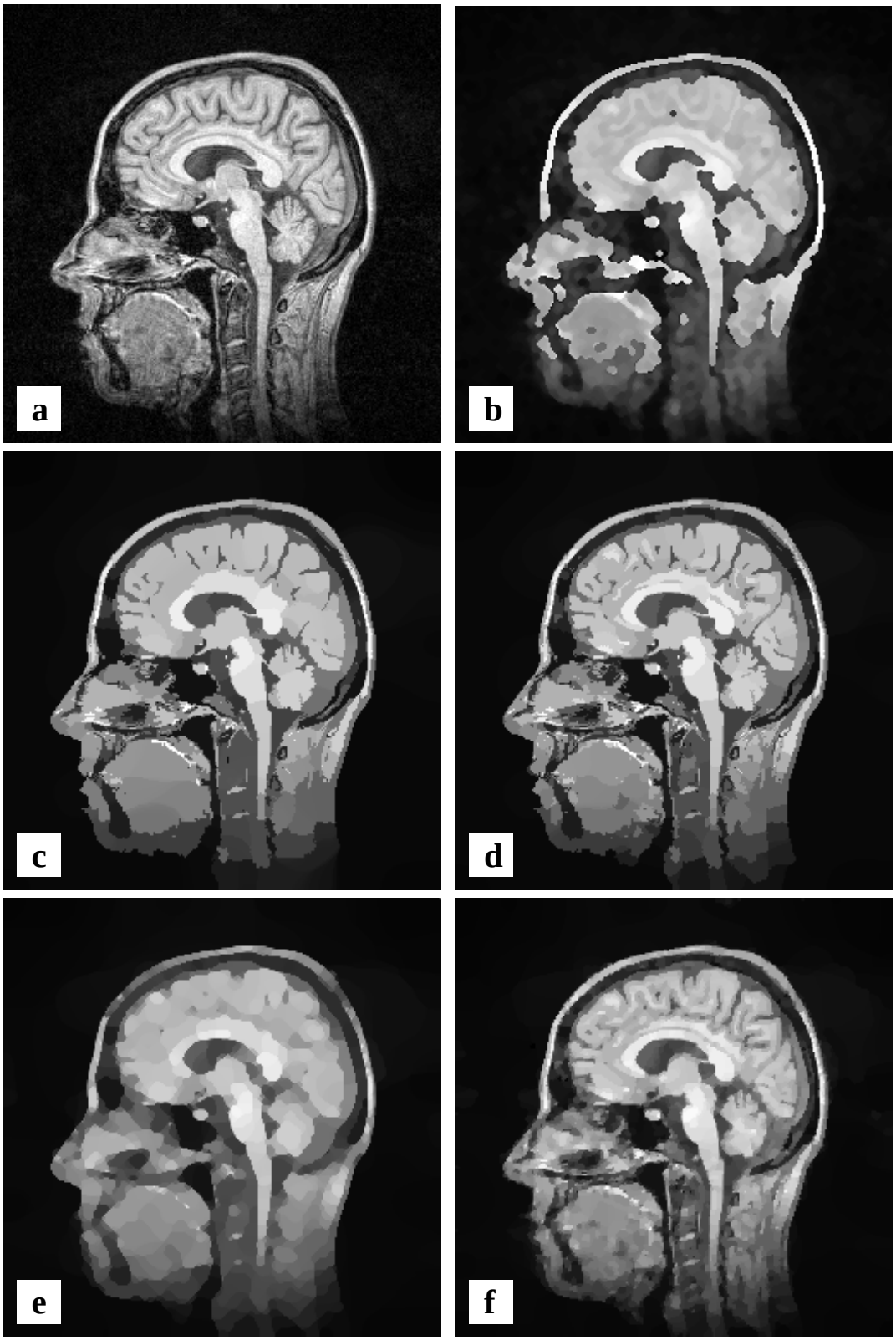

Fig. 6 The ***Head*** experiment. **Top row: (a)** Original image. **(b)** Steady state of iterated median filter. **Middle row: (c)** Iterated AMF, $\varrho = 10$, $\sigma = 0.25$, 10 iterations, L_2 amoeba distance. **(d)** Same but with L_1 amoeba distance. **Bottom row: (e)** Self-snakes with edge-stopping function based on L_1 metric (5), $\sigma = 0.25$, time step size $\tau = 0.25$, 667 iterations. **(f)** Same self-snakes evolution computed on a grid with spatial mesh size 0.25, $\sigma = 0.25$, $\tau = 0.015625$, 10667 iterations.

Table 1 Mean absolute error (MAE) and mean structural similarity index (MSSIM) for amoeba median filtering and self-snakes results of the *Cameraman* experiment. Columns pertain to AMF results with parameters $(\varrho; \sigma;$ iterations), rows belong to self-snakes results with parameters $(\sigma; \tau;$ iterations). Theoretically corresponding pairs are highlighted. Note that the MAE/MSSIM are 1.87/0.950 for Figure 4(a) versus (b), and 2.52/0.954 for Figure 4(c) versus (d).

MAE / MSSIM	Fig. 3(a) (original)	Fig. 4(b) $(10; 0.25; 1)$	Fig. 4(c) $(10; 0.25; 4)$	Fig. 4(d) $(20; 0.25; 1)$	Fig. 4(e) $(20; 0.25; 4)$	Fig. 4(f) $(10; 0.05; 4)$
Fig. 3(a) (original)	0.00 / 1.000	4.43 / 0.850	5.92 / 0.786	6.78 / 0.768	8.73 / 0.730	10.65 / 0.677
Fig. 5(a) $(0.25; 0.25; 67)$	5.28 / 0.810	**2.88 / 0.942**	3.68 / 0.939	4.21 / 0.923	6.36 / 0.893	7.65 / 0.844
Fig. 5(b) $(0.25; 0.25; 267)$	7.25 / 0.754	4.64 / 0.899	**4.35 / 0.926**	**4.34 / 0.924**	5.92 / 0.911	6.26 / 0.879
Fig. 5(c) $(0.05; 0.25; 267)$	9.57 / 0.699	7.08 / 0.845	6.45 / 0.881	5.72 / 0.895	6.32 / 0.906	**4.31 / 0.932**

We contrast the results once more with numerical computations based on the self-snakes PDE, where we use this time the edge-stopping function (25) corresponding to the L_1 amoeba metric (5). A precomputed lookup table with linear interpolation was used for the edge-stopping function.

Since the present test image contains a multitude of small-scale structures, the differences between a conventional PDE discretisation and amoeba median filtering become evident: Figure 6(e) clearly demonstrates an over-simplification due to numerical blurring effects. To give an impression of the influence of the latter, we have re-computed the self-snakes evolution on a finer grid: Using a mesh size of 0.25 instead of 1, the resulting image, Figure 6(f), retains much more structure and shows in the coarser image structures a comparable degree of simplification as the AMF result in Subfigure (d). However, small-scale structures still retain more contrast in the AMF result.

5 Conclusion

In this paper we have presented an analysis of iterated amoeba median filtering which demonstrates that even highly adaptive discrete morphological image filters can be interpreted in terms of PDE-based evolutions. An equivalence result has been proven that links iterated amoeba median filtering to self-snakes, a well-known PDE image filter with segmentation behaviour. Thereby a clear explanation of qualitative properties of iterated AMF was given, together with predictions that could be experimentally checked. Our experiments confirm the predictions of the theoretical investigation, while demonstrating at the same time the difficulties of conventional discretisations of the self-snakes PDE in reproducing its favourable theoretical properties.

It appears therefore attractive to use iterated AMF itself as a discretisation of the self-snakes PDE. Together with equivalence results as by Guichard and Morel this may lead to establishing a dictionary of unconventional discretisations of image filtering PDEs which retain advantageous qualitative characteristics of the PDEs better than standard approaches.

This emphasises a common perspective on discrete and PDE-based image filters, which may help to fuse both formerly disparate branches of image processing.

References

1. L. Alvarez, P.-L. Lions, and J.-M. Morel. Image selective smoothing and edge detection by nonlinear diffusion. II. *SIAM Journal on Numerical Analysis*, 29:845–866, 1992.
2. D. Barash. Bilateral filtering and anisotropic diffusion: towards a unified viewpoint. In M. Kerckhove, editor, *Scale-Space and Morphology in Computer Vision*, volume 2106 of *Lecture Notes in Computer Science*, pages 273–280. Springer, Berlin, 2001.
3. G. Borgefors. Distance transformations in digital images. *Computer Vision, Graphics and Image Processing*, 34:344–371, 1986.
4. G. Borgefors. On digital distance transforms in three dimensions. *Computer Vision and Image Understanding*, 64(3):368–376, 1996.
5. U. M. Braga-Neto. Alternating sequential filters by adaptive neighborhood structuring functions. In P. Maragos, R. W. Schafer, and M. A. Butt, editors, *Mathematical Morphology and its Applications to Image and Signal Processing*, volume 5 of *Computational Imaging and Vision*, pages 139–146. Kluwer, Dordrecht, 1996.
6. R. Carmona and S. Zhong. Adaptive smoothing respecting feature directions. *IEEE Transactions on Image Processing*, 7(3):353–358, Mar. 1998.
7. V. Caselles, J.-M. Morel, and C. Sbert. An axiomatic approach to image interpolation. *IEEE Transactions on Image Processing*, 7(3):376–386, Mar. 1998.
8. C. K. Chui and J. Wang. PDE models associated with the bilateral filter. *Advances in Computational Mathematics*, 2008.
9. S. Didas and J. Weickert. Combining curvature motion and edge-preserving denoising. In F. Sgallari, F. Murli, and N. Paragios, editors, *Scale Space and Variational Methods in Computer Vision*, volume 4485 of *Lecture Notes in Computer Science*, pages 568–579. Springer, Berlin, 2007.
10. E. R. Dougherty and J. Astola, editors. *Nonlinear Filters for Image Processing*. SPIE Press, Bellingham, 1999.
11. R. Fabbri, L. Da F. Costa, J. C. Torelli, and O. M. Bruno. 2D Euclidean distance transform algorithms: a comparative survey. *ACM Computing Surveys*, 40(1):art. 2, 2008.
12. F. Guichard and J.-M. Morel. Partial differential equations and image iterative filtering. In I. S. Duff and G. A. Watson, editors, *The State of the Art in Numerical Analysis*, number 63 in IMA Conference Series (New Series), pages 525–562. Clarendon Press, Oxford, 1997.

13. H. J. A. M. Heijmans. *Morphological Image Operators*. Academic Press, Boston, 1994.
14. J. Hyman, J. Morel, M. Shashkov, and S. Steinberg. Mimetic finite difference methods for diffusion equations. *Computational Geosciences*, 6:333–352, 2002.
15. J. M. Hyman and M. Shashkov. Natural discretizations of the divergence, gradient and curl on logically rectangular grids. *International Journal of Computers and Mathematics with Applications*, 33(4):81–104, 1997.
16. L. Ikonen. Priority pixel queue algorithm for geodesic distance transforms. *Image and Vision Computing*, 25(10):1520–1529, 2007.
17. L. Ikonen and P. Toivanen. Shortest routes on varying height surfaces using gray-level distance transforms. *Image and Vision Computing*, 23(2):133–141, 2005.
18. A. C. Jalba and J. B. T. M. Roerdink. An efficient morphological active surface model for volumetric image segmentation. In M. H. F. Wilkinson and J. B. T. M. Roerdink, editors, *Mathematical Morphology and Its Application to Signal and Image Processing*, volume 5720 of *Lecture Notes in Computer Science*, pages 193–204. Springer, Berlin, 2009.
19. R. Kimmel, N. Sochen, and R. Malladi. Images as embedding maps and minimal surfaces: movies, color, and volumetric medical images. In *Proc. 1997 IEEE Computer Society Conference on Computer Vision and Pattern Recognition*, pages 350–355, San Juan, Puerto Rico, June 1997. IEEE Computer Society Press.
20. R. Klette and P. Zamperoni. *Handbook of Image Processing Operators*. Wiley, New York, 1996.
21. M. Kuwahara, K. Hachimura, S. Eiho, and M. Kinoshita. Processing of RI-angiocardiographic images. In J. K. Preston and M. Onoe, editors, *Digital Processing of Biomedical Images*, pages 187–202. Plenum, New York, 1976.
22. R. Lerallut, E. Decencière, and F. Meyer. Image processing using morphological amoebas. In C. Ronse, L. Najman, and E. Decencière, editors, *Mathematical Morphology: 40 Years On*, volume 30 of *Computational Imaging and Vision*. Springer, Dordrecht, 2005.
23. R. Lerallut, E. Decencière, and F. Meyer. Image filtering using morphological amoebas. *Image and Vision Computing*, 25(4):395–404, 2007.
24. G. Matheron. *Eléments pour une théorie des milieux poreux*. Masson, Paris, 1967.
25. R. E. Mickens. *Nonstandard Finite Difference Models of Differential Equations*. World Scientific, Singapore, 1994.
26. M. Nagao and T. Matsuyama. Edge preserving smoothing. *Computer Graphics and Image Processing*, 9(4):394–407, Apr. 1979.
27. G. Sapiro. Vector (self) snakes: a geometric framework for color, texture and multiscale image segmentation. In *Proc. 1996 IEEE International Conference on Image Processing*, volume 1, pages 817–820, Lausanne, Switzerland, Sept. 1996.
28. J. Serra. *Image Analysis and Mathematical Morphology*, volume 1. Academic Press, London, 1982.
29. J. Serra. *Image Analysis and Mathematical Morphology*, volume 2. Academic Press, London, 1988.
30. C. Tomasi and R. Manduchi. Bilateral filtering for gray and color images. In *Proc. Sixth International Conference on Computer Vision*, pages 839–846, Bombay, India, Jan. 1998. Narosa Publishing House.
31. J. W. Tukey. *Exploratory Data Analysis*. Addison–Wesley, Menlo Park, 1971.
32. R. van den Boomgaard. Decomposition of the Kuwahara–Nagao operator in terms of linear smoothing and morphological sharpening. In H. Talbot and R. Beare, editors, *Mathematical Morphology: Proc. Sixth International Symposium*, pages 283–292, Sydney, Australia, Apr. 2002. CSIRO Publishing.
33. J. G. Verly and R. L. Delanoy. Adaptive mathematical morphology for range imagery. *IEEE Transactions on Image Processing*, 2(2):272–275, 1993.
34. Z. Wang, A. C. Bovik, H. R. Sheikh and E. P. Simoncelli. Image quality assessment: From error visibility to structural similarity. *IEEE Transactions on Image Processing*, 13(4):600–612, 2004.
35. M. Welk, M. Breuß, and O. Vogel. Differential equations for morphological amoebas. In M. H. F. Wilkinson and J. B. T. M. Roerdink, editors, *Mathematical Morphology and Its Application to Signal and Image Processing*, volume 5720 of *Lecture Notes in Computer Science*, pages 104–114. Springer, Berlin, 2009. – Erratum: `http://www.mia.uni-saarland.de/publications`
36. R. T. Whitaker and X. Xue. Variable-conductance, level-set curvature for image denoising. In *Proc. 2001 IEEE International Conference on Image Processing*, pages 142–145, Thessaloniki, Greece, Oct. 2001.
37. A. Yezzi Jr. Modified curvature motion for image smoothing and enhancement. *IEEE Transactions on Image Processing*, 7(3):345–352, Mar. 1998.